back-bonding, this result would imply that equatorial back-bonding in $FeOEP(py)_2$ is larger than that in $OsOEP(py)_2$. This conclusion seems highly improbable. In addition, ν_4 of $OsOEP(py)_2$ is downshifted 9 cm^{-1} from that of OsOEP(CO)(py) whereas ν_4 of $OsOEP(NH_3)_2$ is downshifted 11 cm^{-1} from that of $OsOEP(py)_2$. The shifts for the analogous Fe complexes are 14 and 8 cm^{-1}, respectively. The reversal in the ordering of the ν_4 shifts of the Os(II) versus Fe(II) complexes again suggests that the frequency of ν_4 is reduced by equatorial back-bonding. Collectively, these results suggest that the similarity between the observed and calculated frequencies of ν_4 for OsOEP(CO)(py) is fortuitous. This seems all the more likely considering that the frequency of the ν_4 mode of Ru(OEP)(CO)(py) is 1371 cm^{-1}, which is lower than that of ν_4 of Os(OEP)(CO)(py) (1374 cm^{-1}). It should also be noted that the correlation coefficient for the ν versus C_t-N plot of the ν_4 mode ($r \sim 0.7$) of metallo-OEP complexes is much less satisfying than those obtained for the other high-frequency skeletal modes ($r \sim 0.95$). The poor correlation coefficient for the ν_4 mode is in large part due to the fact that metallo-OEP complexes with large core sizes deviate the most from the straight line generated by least-squares fitting of the data. Given this fact, the ν_4 mode is probably best used only as an indicator of the extent of equatorial back-bonding in different axial ligand adducts of a given metal ion. Thus, the ν_{11} mode appears to be the most reliable indicator of the extent of equatorial back-bonding in metalloporphyrins in general.

Acknowledgment. This work was supported by Grant GM-36243 from the National Institute of General Medical Sciences.

Registry No. OsOEP(CO)(py), 51286-85-2; $OsOEP(py)_2$, 51286-87-4; $OsOEP(NH_3)_2$, 72099-11-7; $FeOEP(py)_2$, 19496-63-0; $FeOEP(NH_3)_2$, 61095-78-1.

Contribution from the Department of Chemistry, University of Houston, Houston, Texas 77004, and Laboratoire de Synthèse et d'Electrosynthèse Organométallique, Associé au CNRS (UA 33), Faculté des Sciences "Gabriel", University of Dijon, 21100 Dijon, France

Synthesis and Reactivity of σ-Bonded Silicon Metalloporphyrins. Spectroscopic Characterization and Electrochemistry of $(P)Si(R)_2$, (P)Si(R)X, and $(P)SiX_2$, Where R = C_6H_5 or CH_3 and X = OH^- or ClO_4^-

K. M. Kadish,*[1a] Q. Y. Xu,[1a] J.-M. Barbe,[1a,b] and R. Guilard*[1b]

Received May 4, 1987

The synthesis, characterization, and electrochemistry of several $(OEP)Si(R)_2$, (OEP)Si(R)X, and $(OEP)SiX_2$ complexes are reported, where OEP is the dianion of octaethylporphyrin, R is C_6H_5 or CH_3, and X = ClO_4^- or OH^-. $(OEP)Si(C_6H_5)_2$ can be converted to $(OEP)Si(C_6H_5)OH$ in $CHCl_3$ by irradiation with visible light in the absence of oxygen. Each Si(IV) complex undergoes a reversible electroreduction at the porphyrin π ring system. In contrast, the initial electrooxidations of these complexes are irreversible and the overall processes involve one or more coupled chemical reactions following electron transfer. $(OEP)Si(C_6H_5)_2$ can be converted to $(OEP)Si(C_6H_5)OH$ after oxidation by one electron while further oxidation generates $(OEP)Si(C_6H_5)ClO_4$. The latter compound can also be formed by reaction of $(OEP)Si(C_6H_5)_2$ with 2 equiv of $HClO_4$ in PhCN. $(OEP)Si(CH_3)_2$ undergoes electrochemistry different from that of $(OEP)Si(C_6H_5)_2$ and gives $(OEP)Si(CH_3)ClO_4$ and $(OEP)Si(ClO_4)_2$ as successive electrooxidation products. An overall oxidation/reduction scheme for $(OEP)Si(R)_2$ is presented and compared to mechanisms for oxidation/reduction of (OEP)Si(R)X and $(OEP)SiX_2$.

Introduction

Non-transition-metal porphyrins with σ-bonded ligands have been reported for Ga, In, and Tl in group 13 and for Ge and Sn in group 14 of the periodic table.[2] Of these compounds, the synthesis and spectroscopic properties of σ-bonded germanium and tin dialkyl and diaryl porphyrins have been the most extensively studied.[3-9] Our laboratories have also recently completed a chemical and electrochemical investigation of $(P)Ge(R)_2$ and (P)Ge(R)X, where P = the dianion of the tetraphenylporphyrin (TPP) or octaethylporphyrin (OEP), R = CH_3, $CH_2C_6H_5$, or C_6H_5 and X = Cl^-, OH^-, or ClO_4^-.[10] This work is a continuation of our synthetic and electrochemical/spectroscopic studies on group 14 metalloporphyrins and reports the electrochemistry of $(OEP)Si(R)_2$, (OEP)Si(R)OH, and $(OEP)Si(OH)_2$, where R = C_6H_5 or CH_3. We also give preliminary data on the electrochemistry of $(OEP)Si(C_6H_5)ClO_4$. No characterization of a dialkyl or diaryl σ-bonded silicon porphyrin has ever been reported nor has an electrochemical study of any silicon porphyrin ever been published. As will be shown in this paper, the electrochemistry of σ-bonded Si(IV) metalloporphyrins is similar to but not identical with that of the related σ-bonded Ge(IV) derivatives.

Experimental Section

$(OEP)Si(C_6H_5)_2$ and $(OEP)Si(CH_3)_2$ were synthesized by using the same method employed for preparation of dialkyl- and diarylgermanium porphyrins.[10] Characterization of each complex was achieved by ^1H NMR, IR, UV-visible spectroscopies, mass spectrometry, and elemental analysis. The $(OEP)Si(R)_2$ complexes are sensitive to both oxygen and visible light. Therefore, all electrochemical measurements were carried

(1) (a) University of Houston. (b) University of Dijon.
(2) Guilard, R.; Lecomte, C.; Kadish, K. M. *Struct. Bonding (Berlin)* **1987**, *64*, 205-268.
(3) Maskasky, J. E.; Kenney, M. E. *J. Am. Chem. Soc.* **1971**, *93*, 2060.
(4) Maskasky, J. E.; Kenney, M. E. *J. Am. Chem. Soc.* **1973**, *95*, 1443.
(5) Cloutour, C.; Lafargue, D.; Richards, J. A.; Pommier, J. C. *J. Organomet. Chem.* **1977**, *137*, 157.
(6) Cloutour, C.; Debaig-Valade, C.; Pommier, J. C.; Dabosi, G.; Martineau, M. *J. Organomet. Chem.* **1981**, *220*, 21.
(7) Cloutour, C.; Lafargue, D.; Pommier, J. C. *J. Organomet. Chem.* **1983**, *190*, 35.
(8) Cloutour, C.; Debaig-Valade, C.; Gacherieu, C.; Pommier, J. C. *J. Organomet. Chem.* **1984**, *269*, 239.
(9) Cloutour, C.; Lafargue, D.; Pommier, J. C. *J. Organomet. Chem.* **1978**, *161*, 329.
(10) Kadish, K. M.; Xu, Q. Y.; Barbe, J.-M.; Anderson, J. E.; Wang, E.; Guilard, R. *J. Am. Chem. Soc.* **1987**, *109*, 7705.

0020-1669/88/1327-1191$01.50/0

Table I. UV–Visible Data for $(OEP)Si(R)_2$ (R = CH_3 or C_6H_5), $(OEP)Si(C_6H_5)OH$, and $(OEP)Si(OH)_2$ in PhCN

compd	λ, nm (ε × 10^{-4}, M^{-1} cm^{-1})					
	N(0,0)	B(1,0)	B(0,0)	Q(2,0)	Q(1,0)	Q(0,0)
$(OEP)Si(CH_3)_2$	349 (4.93)	430 (8.24)	443 (29.12)	528 (0.34)	571 (1.60)	606 (0.24)
$(OEP)Si(C_6H_5)_2$	355 (4.18)	433 (5.93)	446 (27.19)	529 (0.32)	571 (1.58)	606 (0.26)
$(OEP)Si(C_6H_5)OH$	353 (4.61)	407 (5.29)	429 (19.25)	483 (0.16)	552 (1.61)	588 (0.78)
$(OEP)Si(OH)_2$		389 (4.87)	407 (26.88)	471 (0.10)	536 (1.26)	572 (1.38)
$(OEP)SiCl_2$[a]		388 (6.33)	408 (25.80)	502 (0.10)	537 (1.42)	575 (1.54)

[a] Starting material in synthesis of above σ-bonded complexes.

out in darkness and in a drybox. Elemental analyses were obtained from the Service Central de Microanalyses du CNRS. ^1H NMR spectra were recorded at 300 MHz on a Nicolet NT-300 spectrometer controlled by a Model 293.C programmer. Spectra were measured on solutions of 3 mg of complex in $CDCl_3$ with tetramethylsilane used as internal reference. IR spectra were performed by using an IBM FTIR 32 spectrometer coupled with an IBM Model 9000 microcomputer. Samples were prepared as 1% dispersions in CsI. Electronic absorption spectra were recorded on either a Perkin-Elmer 559 spectrophotometer, an IBM Model 9430 spectrophotometer, or a Tracor Northern 1710 holographic optical spectrometer multichannel analyzer. Mass spectra were recorded in the electron-impact mode with a Finnigan 3300 spectrometer: ionizing energy, 70 eV; ionizing current, 0.4 mA; source temperature, 250–400 °C. The photochemical synthesis was carried out under argon by using a visible OSRAM 100-W source.

Cyclic voltammetric measurements were obtained with either an IBM EC225 voltammetric analyzer or an EG&G Princeton Applied Research Model 174A/175 polarographic analyzer/potentiostat. This latter instrument was coupled with an EG&G Model 9002A X-Y recorder for potential scan rates equal to or smaller than 500 mV/s. ESR spectra were recorded on an IBM Model ER 100D electron spin resonance system.

A three-electrode system, which consisted of platinum working and counter electrodes, was used for electrochemical measurements. A platinum minigrid electrode was used in the thin-layer spectroelectrochemical cell. A saturated calomel electrode (SCE) was used as the reference electrode and was separated from the bulk of the solution by a fritted-glass disk junction. Bulk controlled-potential coulometry was carried out with an EG&G Princeton Applied Research Model 173 potentiostat/Model 179 coulometer system, coupled with an EG&G Model RE 0074 time-base X-Y recorder. Thin-layer spectroelectrochemical measurements were made with an IBM EC225 voltammetric analyzer coupled with a Tracor Northern 1710 spectrometer/multichannel analyzer.

Chemicals. Synthesis of $(OEP)Si(OH)_2$ and the $(OEP)SiCl_2$ starting material were carried out by using literature methods.[11] Toluene was dried and distilled from sodium–benzophenone under argon prior to use. Chloroform ($CHCl_3$) was distilled from sodium sulfate under nitrogen. Reagent grade benzonitrile (PhCN) was vacuum-distilled from P_2O_5 while spectroanalytical grade methylene chloride (CH_2Cl_2) was distilled over CaH_2 under argon prior to use. Tetra-*n*-butylammonium perchlorate (TBAP) was purchased from Eastman Kodak Co., purified by two recrystallizations from ethyl alcohol, and stored in a vacuum oven at 40 °C.

Preparation of $(OEP)Si(R)_2$, Where R = CH_3 and C_6H_5. All syntheses were performed under argon by using Schlenk techniques. $(OEP)Si(R)_2$ complexes were synthesized by using a procedure described for synthesis of $(P)Ge(R)_2$.[10] The resulting compounds were recrystallized in toluene and gave yields close to 50%.[12]

Preparation of $(OEP)Si(C_6H_5)OH$. Irradiation of $(OEP)Si(C_6H_5)_2$ (0.33 g, 0.55 mmol) in 400 mL of $CHCl_3$ for 24 h led to the formation of $(OEP)Si(C_6H_5)OH$ (0.30 g; yield = 85%). The purity of the isolated compound was checked by UV–visible, ^1H NMR, and IR spectroscopies. Attempts to prepare the monomethyl derivative by using the same procedure were unsuccessful, and the final isolated compound was invariably $(OEP)Si(OH)_2$, which resulted from cleavage of the two Si–C bonds of $(OEP)Si(CH_3)_2$.

Results and Discussion

Spectroscopic Properties of $(OEP)Si(R)_2$ and $(OEP)Si(C_6H_5)OH$, Where R = C_6H_5 and CH_3. Spectroscopic properties

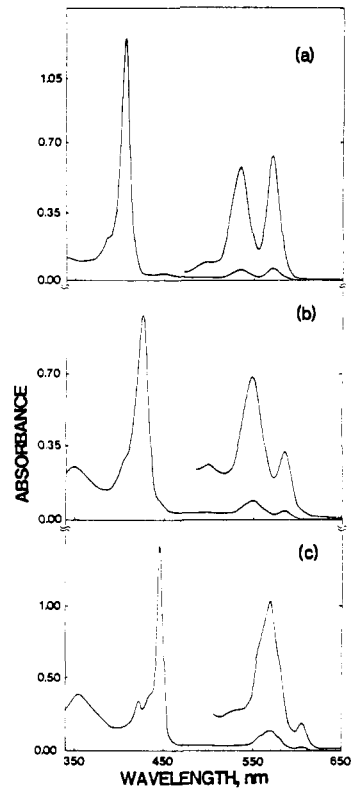

Figure 1. Electronic absorption spectra of (a) $(OEP)Si(OH)_2$, (b) $(OEP)Si(C_6H_5)OH$, and (c) $(OEP)Si(C_6H_5)_2$ in PhCN.

Table II. IR Data (cm^{-1}) for $(OEP)Si(R)_2$, $(OEP)Si(C_6H_5)OH$, and $(OEP)Si(OH)_2$

compd[a]	ν_{O-H}	ν_{C-H}	ν_{Si-OH}	ν_{Si-C}
$(OEP)Si(CH_3)_2$		2900		700
$(OEP)Si(C_6H_5)_2$		3070, 3050, 3030		505
$(OEP)Si(C_6H_5)OH$	3677	3063, 3040	756	424
$(OEP)Si(OH)_2$	3665		835	

[a] CsI pellets.

of $(OEP)Si(R)_2$ are close to those of $(OEP)Ge(R)_2$ containing the same R group. Elemental analysis[12] and mass spectral data[13] confirm the presence of two silicon–carbon bonds. Furthermore, the parent peaks in the mass spectrum are the monomethyl and monophenyl derivatives, which illustrates the facile cleavage of one silicon–carbon bond of $(OEP)Si(R)_2$.

A summary of electronic absorption spectral data for $(OEP)Si(CH_3)_2$ and $(OEP)Si(C_6H_5)_2$ is given in Table I while Figure 1 shows the spectra of $(OEP)Si(OH)_2$, $(OEP)Si(C_6H_5)OH$, and $(OEP)Si(C_6H_5)_2$ in PhCN. Similar spectral properties are observed for $(OEP)Si(CH_3)_2$ and $(OEP)Si(C_6H_5)_2$ (see Table I). The Soret band of the mono-σ-bonded $(OEP)Si(C_6H_5)OH$ derivative (band B(0,0) in Table I) appears at 429 nm, which is

(11) Buchler, J. W.; Puppe, L.; Rohbock, K.; Schneehage, H. H. *Chem. Ber.* **1973**, *106*, 2710.

(12) Anal. Found (calcd) for $C_{48}H_{54}N_4Si$ ($(OEP)Si(C_6H_5)_2$): C, 80.5 (80.84); H, 7.6 (7.65); N, 7.6 (7.57). Good analytical results could not be obtained for $(OEP)Si(CH_3)_2$ due to its instability.

(13) Mass spectral data for $(OEP)Si(CH_3)_2$ [ion, *m/e* (intensity, %)]: $[(OEP)Si(CH_3)_2]^{+\cdot}$, 590 (49.25); $[(OEP)Si(CH_3)]^+$, 575 (100.00). $[(OEP)Si]^+$, 560 (16.29). Data for $(OEP)Si(C_6H_5)_2$ [ion, *m/e* (intensity, %)]: $[(OEP)Si(C_6H_5)_2]^{+\cdot}$, 714 (1.79); $[(OEP)Si(C_6H_5)]^+$, 637 (100.00); $[(OEP)Si]^+$, 560 (1.15).

Table III. ^{1}H NMR Data for (OEP)Si(R)$_2$ (R = CH_3 or C_6H_5), (OEP)Si(C_6H_5)OH, and (OEP)Si(OH)$_2$ in $CDCl_3$[a]

	protons of macrocycle						protons of axial ligands			
compd	mult/i	$\delta(-CH_2-)$	mult/i	$\delta(-CH_3)$	mult/i	δ(methinic H)	mult/i	$\delta(M-CH_3)$ or $\delta(M-C_6H_5)$	mult/i	δ(M–OH)
(OEP)Si(CH_3)$_2$	q/16	4.13	t/24	1.96	s/4	10.09	s/6	−8.16		
(OEP)Si(C_6H_5)$_2$	q/16	3.99	t/24	1.85	s/4	9.75	d/4	0.12		
							t/4	4.53		
							t/2	5.12		
(OEP)Si(C_6H_5)OH	m/16	4.03	t/24	1.90	s/4	9.88	d/2	0.08	s/1	−7.44
							t/2	4.55		
							t/1	5.14		
(OEP)Si(OH)$_2$	q/16	4.08	t/24	1.95	s/4	10.02			not detected	

[a] Key: mult = multiplicity, s = singlet, d = doublet, t = triplet, q = quartet, m = multiplet.

Table IV. Half-Wave Potentials (V vs SCE) for Oxidation and Reduction of (OEP)Si(R)$_2$, (OEP)Si(C_6H_5)OH, and (OEP)Si(OH)$_2$ in PhCN Containing 0.1 M TBAP

	oxidn				redn
complex	1st	2nd	3rd[a]	4th[a]	1st
(OEP)Si(OH)$_2$	0.92	1.39			−1.43
(OEP)Si(C_6H_5)OH	0.86[b]	1.14[b]	1.16	1.45	−1.43
(OEP)Si(C_6H_5)$_2$	0.80[b]		1.15	1.45	−1.42
(OEP)Si(CH_3)$_2$	0.72[b]	1.12[b]	1.20	1.45	−1.46

[a] Half-wave potential of electrochemically generated species. [b] E_{pa} measured at 0.1 V/s.

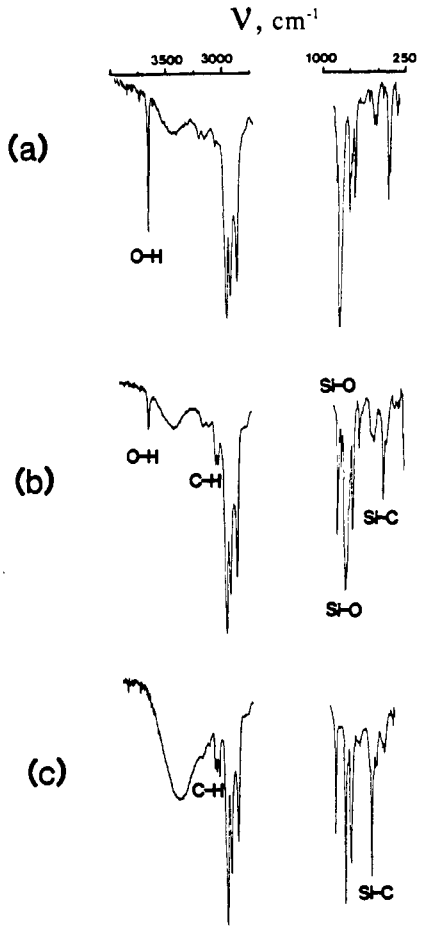

Figure 2. Infrared spectra of (a) (OEP)Si(OH)$_2$, (b) (OEP)Si(C_6H_5)-OH, and (c) (OEP)Si(C_6H_5)$_2$ in CsI pellets.

between the Soret band of (OEP)Si(C_6H_5)$_2$ at 446 nm and that of (OEP)Si(OH)$_2$ at 407 nm. The spectrum of (OEP)Si(C_6H_5)$_2$ is similar to that of (OEP)Ge(C_6H_5)$_2$,[10] and there is an approximate 40-nm red shift of all absorption bands in relation to the bands observed for the (OEP)$SiCl_2$ starting material.

Vibrational frequencies for the Si–OH and Si–C_6H_5 groups of (OEP)Si(C_6H_5)OH are observed at 756 and 424 cm^{-1} and are

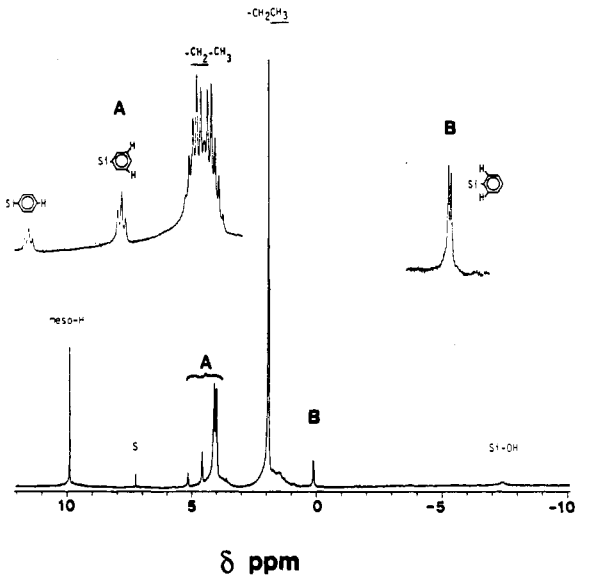

Figure 3. ^{1}H NMR spectrum of (OEP)Si(C_6H_5)OH in $CDCl_3$.

shifted toward lower frequencies by about 80 cm^{-1} with respect to the dihydroxy and diphenyl Si(IV) complexes. These results, as well as IR data for the other Si(IV) complexes, are summarized in Table II. The IR spectra of (OEP)Si(OH)$_2$, (OEP)Si-(C_6H_5)OH, and (OEP)Si(C_6H_5)$_2$ are shown in Figure 2.

^{1}H NMR data for (OEP)Si(CH_3)$_2$ and (OEP)Si(C_6H_5)$_2$ in $CDCl_3$ are listed in Table III. The methylenic protons signal of the macrocycle is a quartet, suggesting that the metal lies in the plane of the porphyrin ring. However, in contrast to the dimethyl and diphenyl complexes, the spectrum of (OEP)Si-(C_6H_5)OH exhibits a multiplet for the methylenic proton resonance signals (see Figure 3). The same behavior is observed for mono-σ-bonded germanium complexes[10] and is explained by the anisotropy of the porphyrin macrocycle enhanced by two different ligands bound to the metal in a trans position. Evidence for the presence of only one phenyl group on (OEP)Si(C_6H_5)OH is also provided by the resonance at −7.44 ppm for the OH proton of (OEP)Si(C_6H_5)OH.

Electrochemistry of (OEP)Si(OH)$_2$. Figure 4a illustrates a cyclic voltammogram of (OEP)Si(OH)$_2$ in PhCN. Two oxidations and one reduction occur within the solvent potential limit. The first oxidation is reversible when the scan direction is reversed at 1.2 V (dashed line, Figure 4a) and conventional voltammetric analysis of the current–voltage curves show this oxidation (labeled process 1) to be a diffusion-controlled reversible one-electron transfer. However, this process is not reversible when the potential scan is swept to potentials positive of +1.2 V (solid line, Figure 4a). Under these conditions a second oxidation is obtained at E_{pa} = 1.34 V (process 2). This oxidation peak is associated with a cathodic rereduction peak at E_{pc} = 1.07 V (process 3).

The above voltammetric behavior suggests that the first oxidation of (OEP)Si(OH)$_2$ involves an EC type mechanism (a chemical reaction following a reversible electron transfer) and this was confirmed by variable scan and multiscan cyclic voltammo-

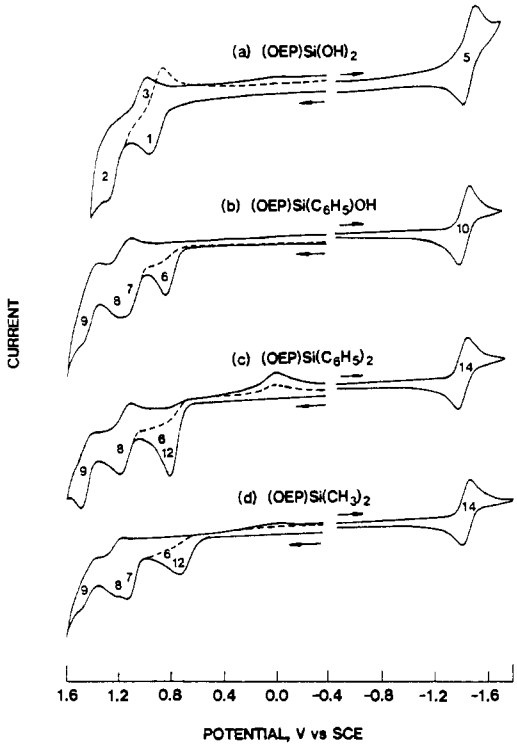

Figure 4. Cyclic voltammograms of (a) 2.0×10^{-3} M $(OEP)Si(OH)_2$, (b) 1.0×10^{-3} M $(OEP)Si(C_6H_5)OH$, (c) 1.0×10^{-3} M $(OEP)Si(C_6H_5)_2$, and (d) 1.0×10^{-3} M $(OEP)Si(CH_3)_2$ in PhCN containing 0.1 M TBAP. Scan rate = 0.1 V/s.

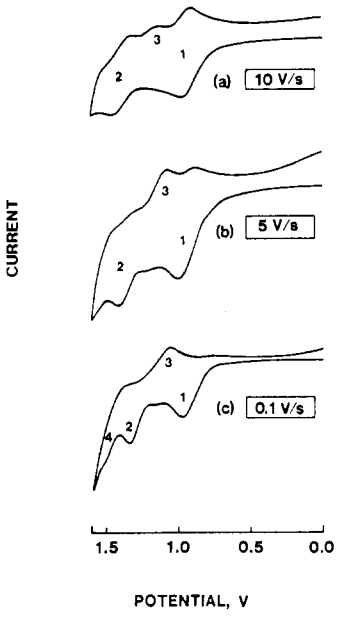

Figure 5. Cyclic voltammograms illustrating the oxidation of 1.0×10^{-3} M $(OEP)Si(OH)_2$ at the following scan rates in PhCN containing 0.1 M TBAP: (a) 10 V/s; (b) 5 V/s; (c) 0.1 V/s.

grams such as those shown in Figure 5. At 10 V/s (Figure 5a) there are two major oxidation/reduction processes (processes 1 and 2). There is also another reduction peak which appears after the potential is scanned to values positive of 1.6 V (peak 3). At 5 V/s (Figure 5b) a cathodic reduction peak is no longer coupled to process 2 but a small reduction peak is still coupled to process 1. This indicates that the chemical reaction following the first and/or second oxidation of $(OEP)Si(OH)_2$ is not complete at this scan rate. Under these conditions, the currents for process 3 have increased in intensity from those observed at 10 V/s. Finally, four processes are observed at 0.1 V/s (Figure 5c). A new oxidation process 4 is observed at the edge of the solvent and both processes 1 and 2 are irreversible due to the chemical reaction following

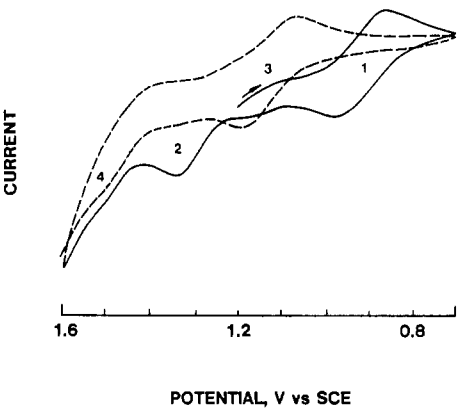

Figure 6. Multiscan cyclic voltammogram of 1×10^{-3} M $(OEP)Si(OH)_2$ in PhCN containing 0.1 M TBAP. Initial potential is 1.2 V.

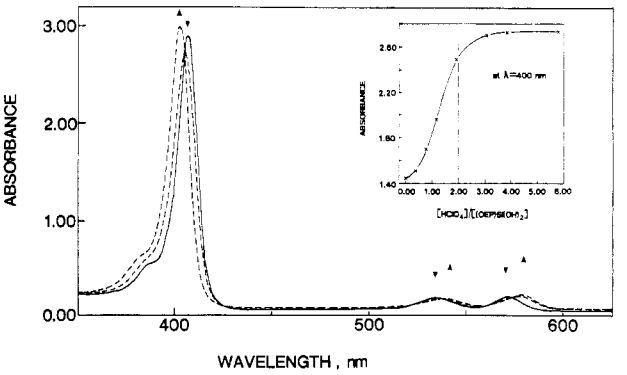

Figure 7. Spectroscopically monitored conversion of $(OEP)Si(OH)_2$ (—) to $(OEP)Si(ClO_4)_2$ (- -) in PhCN. Insert: Spectral changes at $\lambda = 400$ nm as $HClO_4$ is added to the initial solution of $(OEP)Si(OH)_2$.

Scheme I

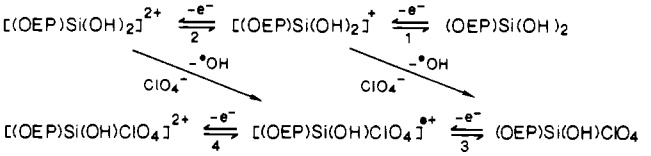

process 1, process 2, or both processes.

The data in Figure 5 indicate that the chemical reactions following oxidation of $(OEP)Si(OH)_2$ generate new species that are involved in processes 3 and 4. A conversion between the electroactive species involved in these processes is also illustrated by the multiscan voltammogram in Figure 6.

In a typical experiment involving $(OEP)Si(OH)_2$ the initial potential was first set at 1.20 V and then negatively scanned to 0.70 V before reversal to +1.6 V. Under these conditions a reversible oxidation is obtained at $E_{1/2} = 0.92$ V (process 1). There is also an irreversible oxidation peak at $E_p = 1.34$ V (process 2) and an irreversible oxidation at $E_p \approx 1.46$ V (process 4). On the second potential scan between +1.6 and +0.7 V (dashed line, Figure 6), both processes 1 and 2 disappear and only processes 3 and 4 remain.

Theoretical calculations suggest that the highest occupied molecular orbital (HOMO) of $(OEP)Si(OH)_2$ is $e_u(O)$ from the OH group,[14] and this orbital is accessible to abstraction of an electron. Furthermore, reversible oxidation potentials can be related to the energy of the HOMO orbital.[15] The abstraction of an electron from the $e_u(O)$ orbital of $(OEP)Si(OH)_2$ would destabilize the Si–O bond so that the OH group will dissociate. This would lead to a heterolytic cleavage of the Si–O bond, generating $(OEP)Si(OH)(ClO_4)$ in solution. This species is indeed

(14) Schaffer, A. M.; Gouterman, M. *Theor. Chim. Acta* **1970**, *18*, 1.
(15) Maccoll, A. *Nature (London)* **1949**, *163*, 178.

Table V. Peak Maximum Wavelengths and Molar Absorptivities of Neutral, Reduced, and Oxidized $(OEP)Si(R)_2$, $(OEP)Si(C_6H_5)OH$, and $(OEP)Si(OH)_2$ in PhCN Containing 0.2 M TBAP[a]

complex	electrode reacn	λ_{max}, nm ($\epsilon \times 10^{-4}$, M^{-1} cm^{-1})			
$(OEP)Si(OH)_2$	none	406 (28.0)		535 (1.2)	571 (1.3)
	1st redn	431 (8.4)		633 (1.1)	823 (0.6)
$(OEP)Si(C_6H_5)OH$	none	429 (16.0)		553 (1.8)	588 (1.0)
	1st oxidn	405 (17.6)		538 (1.5)	578 (1.8)
	2nd oxidn	404 (8.8)	448 (1.3)	642 (0.6)	710 (0.8)
$(OEP)Si(C_6H_5)_2$	none	447 (27.2)		573 (1.5)	...
	1st redn	466 (7.4)		647 (1.0)	834 (0.8)
$(OEP)Si(CH_3)_2$	none	445 (29.1)		574 (1.6)	...
	1st redn	461 (18.9)		...	841 (1.2)

[a] Only major absorptions are given in this table.

observed, and the overall oxidation reactions of $(OEP)Si(OH)_2$ in PhCN can be described as shown in Scheme I. Processes 1–5 in this scheme are given in the cyclic voltammograms of Figures 4–6.

Attempts to monitor the formation of a free OH radical by ESR spin trap materials during electrooxidation were unsuccessful. However, the reaction of $(OEP)Si(OH)_2$ with $HClO_4$ gives $(OEP)Si(ClO_4)_2$ as a final product in PhCN. In a typical experiment the titration of $(OEP)Si(OH)_2$ with $HClO_4$ was monitored by UV–visible spectroscopy. The starting Si(IV) species has a Soret band at 407 nm and two Q bands at 535 and 572 nm. As $HClO_4$ is added to solutions of $(OEP)Si(OH)_2$, the Soret band decreases in peak intensity and blue shifts. At the same time the two Q bands red shift. The final spectrum is obtained after 2 equiv of $HClO_4$ are added (see Figure 7) and is characterized by peaks at 403, 539, and 579 nm. Five well-defined isosbestic points are present at 404, 424, 520, 561, and 571 nm, indicating that only two species, $(OEP)Si(OH)_2$ and $(OEP)Si(ClO_4)_2$, are spectroscopically observed. This suggests that the acid–base reaction shown in Figure 7 is sufficiently rapid such that the intermediate $(OEP)Si(OH)(ClO_4)$ is not present in large quantities.

The single one-electron reduction of $(OEP)Si(OH)_2$ is uncomplicated in PhCN and CH_2Cl_2 and occurs at $E_{1/2} = -1.43$ and -1.40 V, respectively. A value of $E_{1/2} = -1.35$ V has been reported for reduction of $(OEP)Si(OH)_2$ in Me_2SO.[16] The site of electroreduction in Me_2SO was postulated to be at the porphyrin π ring system and was confirmed in this study by thin-layer spectroelectrochemistry in PhCN. Spectral data for the singly reduced $[(OEP)Si(OH)_2]^-$ ion are summarized in Table V.

Electrochemistry of $(OEP)Si(C_6H_5)OH$ in PhCN. The first oxidation (process 6, Figure 4b) occurs at $E_p = 0.86$ V. This process is not reversible, but the shape and height of the oxidation peak are indicative of a diffusion-controlled one-electron transfer ($|E_p - E_{p/2}| = 60$ mV and $i_p/v^{1/2}$ is constant). A chemical reaction follows the initial electrooxidation. By analogy with $(OEP)Si(OH)_2$, this overall irreversible reaction may be assigned as oxidation and subsequent loss of the bound OH^- ligand on $(OEP)Si(C_6H_5)OH$. Loss of the OH^- ligand will generate $[(OEP)Si(C_6H_5)]^+$ or $(OEP)Si(C_6H_5)ClO_4$, one or both of which are oxidized by the two reversible processes 8 and 9. Process 7 is proposed to involve oxidation of the remaining $[(OEP)Si(C_6H_5)OH]^+$, which is not converted to $(OEP)Si(C_6H_5)ClO_4$ on the cyclic voltammetric time scale. $(OEP)Si(C_6H_5)OH$ is also reversibly reduced at $E_{1/2} = -1.43$ V in PhCN containing 0.1 M TBAP (see Figure 4b, process 10).

Electrochemically Monitored Titration of $(OEP)Si(C_6H_5)OH$ with $HClO_4$. The loss of an OH^- ligand after electrooxidation of $(OEP)Si(C_6H_5)OH$ is consistent with voltammetric data obtained during an electrochemically monitored titration of $(OEP)Si(C_6H_5)OH$ with $HClO_4$. Figure 8 illustrates cyclic voltammograms of $(OEP)Si(C_6H_5)OH$ in PhCN containing 0–1 equiv of $HClO_4$. The cyclic voltammogram of $(OEP)Si(C_6H_5)OH$ in PhCN containing 0.1 M TBAP is characterized by a reversible reduction at $E_{1/2} = -1.43$ V (process 10), two irreversible oxidations at $E_p = 0.86$ and 1.14 V (processes 6 and 7), and two reversible oxidations at $E_{1/2} = 1.16$ and 1.45 V (processes 8 and 9). The same set of oxidation/reduction peaks are observed in PhCN containing 0.4 equiv $HClO_4$, but a new reduction peak (process 11) is also observed at $E_p = -0.82$ V. The current for this reduction process increases as the concentration of $HClO_4$ is increased. At the same time, a decrease in current is observed for the two oxidations at $E_p = 0.86$ V (process 6) and 1.14 V (process 7).

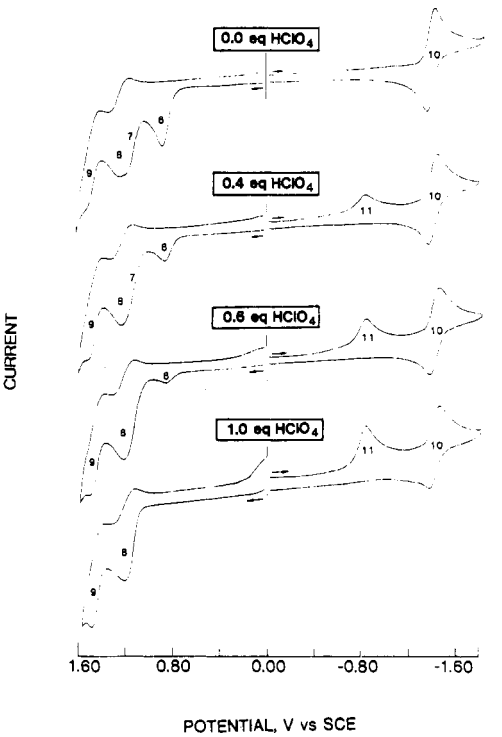

Figure 8. Cyclic voltammograms of 1.43×10^{-3} M $(OEP)Si(C_6H_5)OH$ in PhCN containing 0.1 M TBAP and the following concentrations of $HClO_4$: 0.0 equiv; 0.4 equiv; 0.6 equiv; 1.0 equiv. Scan rate = 0.1 V/s.

The currents for processes 8 and 9 remain unchanged with increasing $HClO_4$ concentration. These processes can be assigned as oxidation of $(OEP)Si(C_6H_5)ClO_4$, which is formed either electrochemically from $(OEP)Si(C_6H_5)OH$ or chemically by the titration of $(OEP)Si(C_6H_5)OH$ with $HClO_4$ (eq 1).

$$(OEP)Si(C_6H_5)OH + HClO_4 \rightleftarrows (OEP)Si(C_6H_5)ClO_4 + H_2O \quad (1)$$

Process 6 is due to oxidation of the bound OH^- on $(OEP)Si(C_6H_5)OH$ while process 11 is due to the reduction of $(OEP)Si(C_6H_5)ClO_4$. The change in peak currents for these two processes as a function of increasing $HClO_4$/porphyrin ratio is shown in Figure 9. As seen in this figure the acid–base reaction given in eq 1 is complete after 1 equiv of $HClO_4$ has been added to the solution. Under these conditions the current for process 11 has reached a maximum and that for process 6 has decreased to zero.

(16) Fuhrhop, J.-H.; Kadish, K. M.; Davis, D. C. *J. Am. Chem. Soc.* **1973**, *95*, 5140.

Scheme II

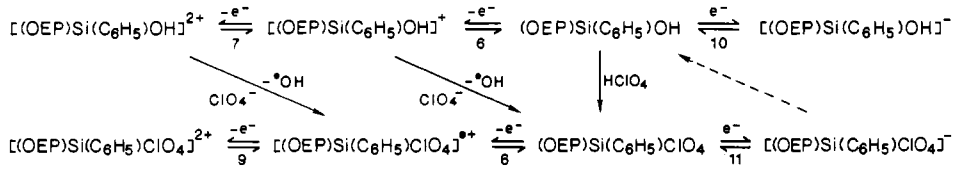

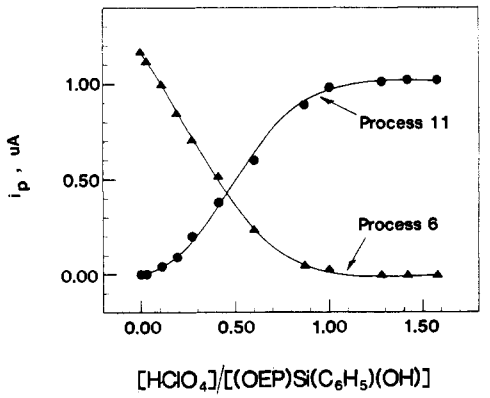

Figure 9. Plot of peak current for process 6 (▲) and process 11 (●) as a function of $[HClO_4]/[(OEP)Si(C_6H_5)OH]$ ratio.

The oxidation of $[(OEP)Si(C_6H_5)OH]^+$ at E_p = 1.14 V (process 7) also disappears as $(OEP)Si(C_6H_5)OH$ is converted to $(OEP)Si(C_6H_5)ClO_4$. The cyclic voltammogram of this latter species is then characterized by oxidations at $E_{1/2}$ = 1.16 and 1.45 V (processes 8 and 9) and reductions at E_{pc} = −0.82 V (process 11) and $E_{1/2}$ = −1.43 V (process 10). The UV–visible spectrum of this solution has a Soret band at 421 nm and two bands at 551 and 588 nm.

As seen in Figure 8, the initial reversible reduction of $(OEP)Si(C_6H_5)OH$ at −1.43 V remains unchanged as $HClO_4$ is added to solution. The reduction at E_p = −0.82 V (process 11) is also irreversible at all concentrations of acid between 0 and 1.0 equiv. If trace water in the solution is reduced by one electron to generate OH^- and H_2, this would result in the conversion of $(OEP)Si(C_6H_5)ClO_4$ to $(OEP)Si(C_6H_5)OH$. This latter species could then be reversibly reduced at $E_{1/2}$ = −1.43 V. These oxidation/reduction processes of $(OEP)Si(C_6H_5)OH$ are summarized in Scheme II. The electron transfer processes 6–11 in this scheme are illustrated by the associated peaks in Figure 8. The above scheme only holds for oxidation/reduction of $(OEP)Si(C_6H_5)OH$ and related species monitored by conventional cyclic voltammetry in PhCN and $PhCN/HClO_4$ mixtures. Different species are observed on the longer thin-layer spectroelectrochemical time scale. This is discussed in the following section.

Spectroelectrochemistry of $(OEP)Si(C_6H_5)OH$ in PhCN. Potential-resolved electronic absorption spectra obtained during electrooxidation of $(OEP)Si(C_6H_5)OH$ in PhCN are shown in Figure 10. The final spectrum after the abstraction of one electron from $(OEP)Si(C_6H_5)OH$ (Figure 10a) is identical with that of $(OEP)Si(ClO_4)_2$.[17] This differs from results by conventional cyclic voltammetry and suggests that both the Si–OH bond and Si–C bond cleave on the thin-layer cyclic voltammetric time scale.

The spectra suggest formation of a porphyrin π cation radical after abstraction of a second electron from $(OEP)Si(C_6H_5)OH$ (Figure 10b). These UV–visible spectral data also indicate that $(OEP)Si(ClO_4)_2$ is initially formed and further suggest that the overall abstraction of two electrons from $(OEP)Si(C_6H_5)OH$ yields $[(OEP)Si(ClO_4)_2]^{\bullet+}$ as a final product on the longer thin-layer spectroelectrochemical time scale.

Electrochemistry of $(OEP)Si(C_6H_5)_2$ and $(OEP)Si(CH_3)_2$ in PhCN. Figure 4c illustrates the cyclic voltammogram of $(OEP)Si(C_6H_5)_2$ in PhCN containing 0.1 M TBAP. The

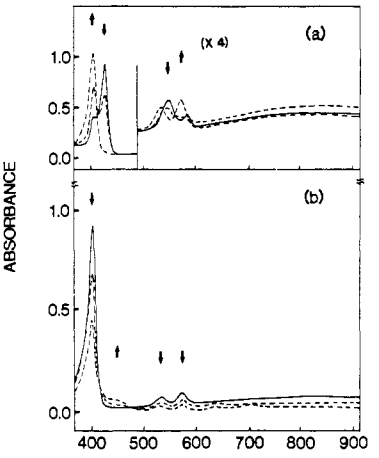

Figure 10. Potential-resolved thin-layer electronic absorption spectra of $(OEP)Si(C_6H_5)OH$ during (a) 1st oxidation and (b) 2nd oxidation in PhCN containing 0.2 M TBAP.

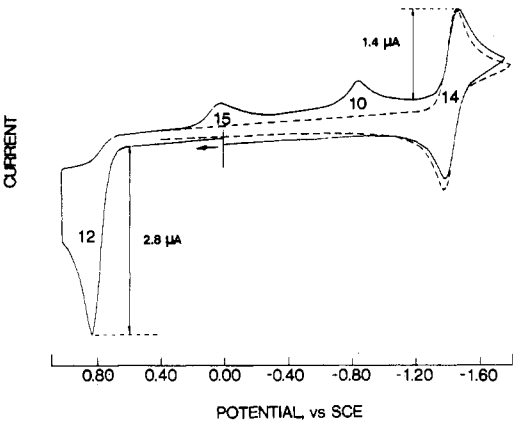

Figure 11. Cyclic voltammogram of 1 × 10^{-3} M $(OEP)Si(C_6H_5)_2$ in PhCN containing 0.1 M TBAP. In one experiment (- -) the scan was varied from +0.40 to −1.60 V. In another experiment (—) the initial scan was varied from 0.0 to 1.0 V and then held at 1.0 V for 5 min before reversing the sweep.

$(OEP)Si(C_6H_5)_2$ complex can be oxidized by a total of four electrons. The first two electrons are abstracted in a single step while the latter two are abstracted in stepwise processes represented by peaks 8 and 9. These latter two oxidations are reversible and have the same half-wave potentials as the third and fourth oxidations of $(OEP)Si(C_6H_5)OH$ (see Figure 4b). This suggests that one Si–C bond of $(OEP)Si(C_6H_5)_2$ cleaves with the formation of $(OEP)Si(C_6H_5)ClO_4$ after the initial two-electron oxidation.

Cyclic voltammograms at a Pt button electrode (Figure 11) and linear sweep voltammograms at a Pt rotating disk electrode indicate that the maximum peak current for the first oxidation of $(OEP)Si(C_6H_5)_2$ (process 12) is twice as high as for the other redox reactions of the same species. The measured $|E_p - E_{p/2}|$ = 60 mV for this process suggests that two one-electron transfers occur at the same potential and are separated by a chemical reaction.

A reduction peak is also observed at −0.82 V when $(OEP)Si(C_6H_5)_2$ is first oxidized at 1.0 V for 5 min and the potential then scanned in a negative direction. This peak is not observed on initial reductive scans of $(OEP)Si(C_6H_5)_2$ (dashed line, Figure

(17) Results for $(OEP)Si(ClO_4)_2$. UV–visible in PhCN [λ nm (ε × 10^{-4}, M^{-1} cm^{-1})]: 383 (7.6), 404 (25.6), 500 (0.2), 537 (1.2), 578 (1.6). IR data (cm^{-1}): ν_{Cl-O}, 1096, 1070, 620; ν_{Si-O}, 399.

Scheme III

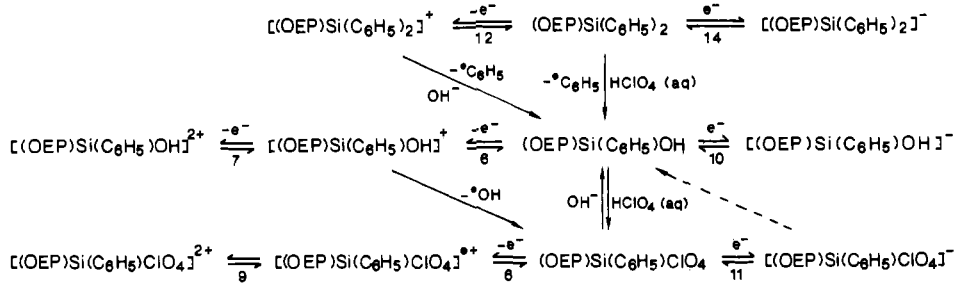

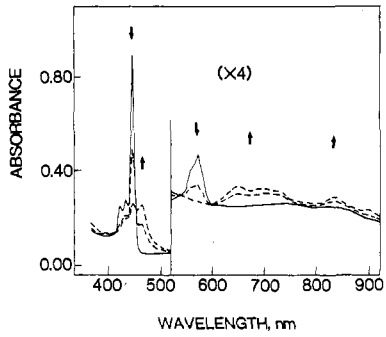

Figure 12. Potential-resolved thin-layer electronic absorption spectra obtained during electroreduction of 2×10^{-5} M $(OEP)Si(C_6H_5)_2$ in PhCN containing 0.2 M TBAP.

11). Comparison of the voltammogram in Figure 11 with the one of $(OEP)Si(C_6H_5)OH$ in PhCN/1.0 equiv $HClO_4$ (Figure 8) suggests that the reaction at $E_p = -0.82$ V can be assigned as reduction of electrogenerated $(OEP)Si(C_6H_5)ClO_4$. An additional reduction peak at ≈0.0 V is also seen after electrooxidation of $(OEP)Si(C_6H_5)_2$ and is assigned as reduction of one or more products of the chemical reaction involving cleavage of the Si–carbon bond.

Unfortunately, changes in the thin-layer electronic absorption spectrum of $(OEP)Si(C_6H_5)_2$ during this two-electron oxidation could not be obtained due to photodecomposition of the complex in the spectrophotometric cell at +0.60 V. As the photodecomposition proceeded, the Soret band at 447 nm first dropped in intensity and shifted to 429 nm. At the same time the bands at 573 nm dropped in intensity while new bands were observed at 553 and 585 nm. This spectrum corresponds to that of $(OEP)Si(C_6H_5)OH$ but all spectral characteristics of this complex are lost after electrooxidation at more positive potentials. Under these conditions the final solution spectrum after electrooxidation corresponds to that of $(OEP)Si(ClO_4)_2$.[17]

A single reduction of $(OEP)Si(C_6H_5)_2$ (process 14) occurs at $E_{1/2} = -1.42$ V and is characterized by $|E_p - E_{p/2}| = 60$ mV, $i_{pa}/i_{pc} = 1.0$ and an $i_p/v^{1/2}$ value that is constant over the scan rate range of 0.05–1.0 V/s. All of these data support the assignment of a diffusion-controlled one-electron transfer.

A reversible reduction of $(OEP)Si(C_6H_5)_2$ is also obtained at a Pt thin-layer electrode, and Figure 12 represents the reversible potential-resolved thin-layer spectral changes obtained in PhCN containing 0.2 M TBAP. The initial σ-bonded species has a Soret band at 447 nm and a Q-band at 573 nm. The final spectrum of the reduction product is characterized by a Soret band at 466 nm and visible bands at 647 and 834 nm and is indicative of a porphyrin π anion radical. These spectral data are summarized in Table V.

Reaction of $(OEP)Si(C_6H_5)_2$ with $HClO_4$. Evidence that the first oxidation of $(OEP)Si(C_6H_5)_2$ consists of two overlapping one-electron transfers (processes 12 and 6) is provided by cyclic voltammograms of $(OEP)Si(C_6H_5)_2$ in PhCN with and without added $HClO_4$. The voltammogram of $(OEP)Si(C_6H_5)_2$ in PhCN containing 0.0, 1.0, and 2.0 equiv of $HClO_4$ is shown in Figure 13a. As seen in this figure, the intensity of processes 12 and 6 are decreased in PhCN containing 1 equiv of $HClO_4$ and in this solution there is a reduction peak at $E_p = -0.82$ V. The cathodic

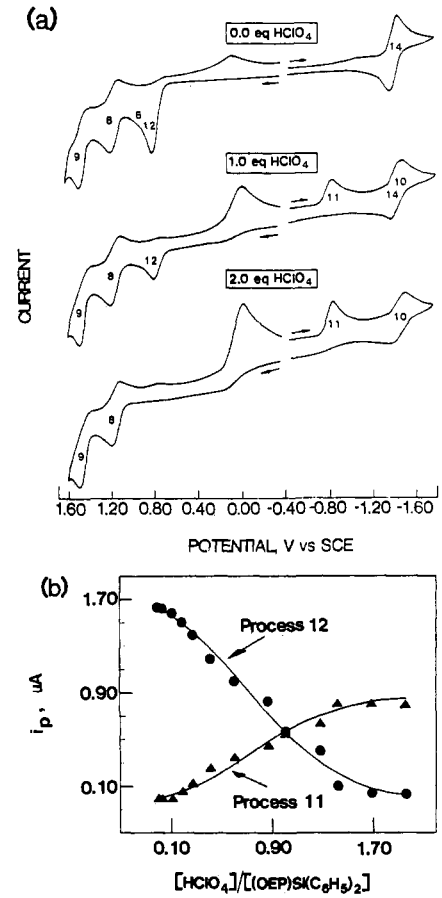

Figure 13. (a) Cyclic voltammograms of $(OEP)Si(C_6H_5)_2$ in solutions containing the following concentrations of $HClO_4$ in PhCN containing 0.1 M TBAP: 0.0 equiv; 1.0 equiv; and 2.0 equiv. (b) Plot of peak currents for processes 11 (▲) and 12 (●) as a function of the $[HClO_4]/[(OEP)Si(C_6H_5)_2]$ ratio.

peak at $E_p \approx 0.0$ V is due to reduction of free H^+ from the excess of $HClO_4$ added to solution.

The first oxidation of $(OEP)Si(C_6H_5)_2$ (process 12) totally disappears in solutions containing 2 equiv of $HClO_4$. The original reduction process 14 shifts negatively by 10 mV upon the addition of 2 equiv of $HClO_4$ while processes 8 and 9 remain at the same potential. The electronic absorption spectrum of the species in PhCN containing 2 equiv of $HClO_4$ is identical with the spectrum of $(OEP)Si(C_6H_5)ClO_4$. This suggests that an electrochemical or chemical conversion of $(OEP)Si(C_6H_5)_2$ to $(OEP)Si(C_6H_5)ClO_4$ has occurred.

Peak currents for processes 11 and 12 are correlated with the $HClO_4$ concentration as shown in Figure 13b. Two equivalents of $HClO_4$ is needed to convert $(OEP)Si(C_6H_5)_2$ to $(OEP)Si(C_6H_5)ClO_4$. Apparently, the first equivalent of acid breaks the Si–carbon bond and generates $(OEP)Si(C_6H_5)OH$ while the second equivalent of $HClO_4$ neutralizes the bound OH^- and forms $(OEP)Si(C_6H_5)ClO_4$.

Electrochemistry of $(OEP)Si(CH_3)_2$. Similar electrochemical behavior is observed for $(OEP)Si(CH_3)_2$ and $(OEP)Si(C_6H_5)_2$

in PhCN but $(OEP)Si(CH_3)_2$ is oxidized at slightly more negative potentials (see Figure 4d). $(OEP)Si(CH_3)_2$ can also be oxidized by four electrons in the potential range of PhCN. The single reversible reduction is diffusion-controlled and occurs at $E_{1/2}$ = −1.46 V. Spectroelectrochemical monitoring of this reaction indicates that the initial product is a porphyrin π anion radical, $[(OEP)Si(CH_3)_2]^-$. These spectral data are given in Table V.

In summary, the oxidative and reductive behaviors of $(OEP)Si(R)_2$ are basically identical for R = CH_3 and C_6H_5. Combining these data with the electrochemistry of $(OEP)Si(C_6H_5)OH$ enables one to derive an overall electrochemical mechanism for all of these complexes. This mechanism is shown in Scheme III for R = C_6H_5.

Comparisons between $(OEP)Si(R)_2$ and $(OEP)Ge(R)_2$. The physicochemical properties of neutral $(OEP)Si(R)_2$ porphyrins are similar to those of $(OEP)Ge(R)_2$.[10] The ^1H NMR, IR, and UV–visible spectroscopies as well as the electrochemical data show this unambiguously.

$(OEP)M(R)ClO_4$ (M = Si or Ge) complexes are oxidized between +1.40 and +1.47 V while the first electrochemical oxidation of $(OEP)M(R)_2$ occurs between +0.72 and +0.88 V. The first oxidation product of $(OEP)M(R)ClO_4$ gives a π cation radical. In contrast, the final product of $(OEP)M(R)_2$ oxidation is not a cation radical due to the rapid cleavage of one metal–carbon bond that occurs after the initial electrochemical oxidation. This instability of the dialkyl and diaryl complexes is related to the site of electron abstraction. The orbital involved in this process could be a σ molecular orbital, i.e., an orbital of the axial ligand that overlaps an orbital of the metal rather than a π ring orbital.

Acknowledgment. The support of the National Science Foundation (Grants No. CHE-8515411 and No. INT-8413696) and the CNRS is gratefully acknowledged.

Registry No. $(OEP)Si(CH_3)_2$, 112896-49-8; $(OEP)Si(C_6H_5)_2$, 112896-50-1; $(OEP)Si(C_6H_5)OH$, 112896-51-2; $(OEP)Si(OH)_2$, 50820-15-0.

Contribution from the Department of Chemistry, University of Houston, Houston, Texas 77004, Laboratoire de Chimie-Physique Générale, Faculté des Sciences de Rabat, Université Mohammed V, Rabat, Morocco, and Laboratoire de Synthèse et d'Electrosynthèse Organometallique, Associé au CNRS (UA 33), Faculté des Sciences "Gabriel", Université de Dijon, 21100 Dijon, France

Electrochemical and Spectroelectrochemical Studies of Nickel(II) Porphyrins in Dimethylformamide

K. M. Kadish,*[1a] D. Sazou,[1a] Y. M. Liu,[1a] A. Saoiabi,[1b] M. Ferhat,[1b] and R. Guilard*[1c]

Received July 8, 1987

The electrochemistry of $(P)Ni^{II}$ in DMF is reported where P is the dianion of tetrapyridylporphyrin (TpyP), tetrakis(*p*-(sodiosulfonato)phenyl)porphyrin (T(*p*-SO_3Na)PP), and tetrakis(*p*-diethylaminophenyl)porphyrin (T(*p*-Et_2N)PP). Each electrode reaction was monitored by cyclic voltammetry, rotating-disk voltammetry, spectroelectrochemistry, and ESR spectroscopy, and on the basis of these data, an overall oxidation–reduction mechanism for each complex is presented. All three compounds can be reduced by one electron to form π anion radicals or oxidized by one or two electrons to form π cation radicals and dications. Additional oxidations are also associated with the diethylamino groups on (T(*p*-Et_2N)PP)Ni. Reduced (T(*p*-SO_3Na)PP)Ni and (T(*p*-Et_2N)PP)Ni are stable, but (TpyP)Ni undergoes demetalation after reduction by two electrons at the porphyrin π ring system. This is the first example for demetalation of an electroreduced nickel porphyrin and contrasts with results for other nickel porphyrins, which are quite stable after electroreduction. The effect of porphyrin ring structure on the electrochemical behavior of each complex is discussed and compared with that of other related metalloporphyrins.

Introduction

The electrochemical reactions of synthetic nickel porphyrins have been characterized in various nonaqueous solvent/supporting electrolyte combinations, and numerous details regarding redox potentials and the site of electron transfer have been presented.[2-9] Studies of nickel porphyrins are of interest with respect to their biological relevance[10-12] and to the fact that they are found in shale oils.[13] In this regard, nickel and vanadyl porphyrins are the main organic geochemical constituents in fossil plant material.[14,15]

The spectroscopic and physical properties of several tetrapyridylporphyrins and tetrakis(*p*-sulfonatophenyl)porphyrins have been investigated.[6,16-22] In the present study we report the electrochemistry and spectroelectrochemistry of (TpyP)Ni, (T(*p*-SO_3Na)PP)Ni, and (T(*p*-Et_2N)PP)Ni in DMF. Structures of these three nickel complexes are shown in Figure 1.

The electrochemistry of (TpyP)Ni and (T(*p*-SO_3Na)PP)Ni has not been reported in the literature, but that of (T(*p*-Et_2N)PP)Ni in CH_2Cl_2 is known.[2] This compound undergoes one reduction and either two or three oxidations depending upon the solvent and supporting electrolyte system. The complex is oxidized at $E_{1/2}$ = 0.63 and 1.11 V and reduced at −1.36 V in CH_2Cl_2 when TBAP is used as the supporting electrolyte.[2] A third oxidation of (T(*p*-Et_2N)PP)Ni is also observed at $E_{1/2}$ = 1.4 V when $TBA(PF_6)$ is used as the supporting electrolyte. Identical reductive behavior is observed in CH_2Cl_2 and DMF, but the oxidative properties are quite different in these two solvents containing 0.1 M TBAP. Mechanisms for reduction and oxidation of the three complexes

(1) (a) University of Houston. (b) Université Mohammed V. (c) Université de Dijon.
(2) Chang, D.; Malinski, T.; Ulman, A.; Kadish, K. M. *Inorg. Chem.* **1984**, *23*, 817.
(3) Wolberg, A.; Manassen, J. *Inorg. Chem.* **1970**, *9*, 2365.
(4) Wolberg, A.; Manassen, J. *J. Am. Chem. Soc.* **1970**, *92*, 2982.
(5) Dolphin, D.; Niem, T.; Felton, R. H.; Fajita, S. *J. Am. Chem. Soc.* **1975**, *97*, 5288.
(6) Johnson, E. E.; Niem, T.; Dolphin, D. *Can. J. Chem.* **1978**, *56*, 1381.
(7) Kadish, K. M.; Morrison, M. M. *Inorg. Chem.* **1976**, *15*, 980.
(8) Felton, R. H.; Linschitz, H. *J. Am. Chem. Soc.* **1966**, *88*, 1113.
(9) Kadish, K. M.; Morrison, M. M. *Bioinorg. Chem.* **1977**, *7*, 107.
(10) Ellefson, W. L.; Whitman, W. B.; Wolfe, R. S. *Proc. Natl. Acad. Sci. U.S.A.* **1982**, *79*, 3707.
(11) Livingston, D. A.; Pfaltz, A.; Schreiber, J.; Eschenmoser, A.; Ankel-Fuchs, D.; Moll, J.; Jaenchen, R.; Thauer, R. K. *Helv. Chim. Acta* **1984**, *67*, 334.
(12) Pfaltz, A.; Livingston, D. A.; Jaun, B.; Diekert, G.; Thauer, R. K.; Eschenmoser, A. *Helv. Chim. Acta* **1985**, *68*, 1338.
(13) Saoiabi, A.; Ferhat, M.; Barbe, J.-M.; Guilard, R. *Fuel* **1983**, *62*, 963.
(14) Baker, E. W.; Palmer, S. E. In *The Porphyrins*; Dolphin, D., Ed.; Academic: New York, 1978; Vol. 1A, Chapter 11, p 485.
(15) Dickson, F. E.; Petrakis, L. *J. Phys. Chem.* **1970**, *74*, 2850.
(16) Neri, B. P.; Wilson, G. S. *Anal. Chem.* **1973**, *45*, 442.
(17) Williams, R. F. X.; Hambright, P. *Bioinorg. Chem.* **1978**, *9*, 537.
(18) Pasternack, R. F. *Ann. N.Y. Acad. Sci.* **1973**, *206*, 614.
(19) Pasternack, R. F.; Francesconi, L.; Raff, D.; Spiro, E. *Inorg. Chem.* **1973**, *12*, 2606.
(20) Kalyanasundaram, K. *Inorg. Chem.* **1984**, *23*, 2453.
(21) Brookfield, R. L.; Ellul, H.; Harriman, A. *J. Photochem.* **1985**, *31*, 97.
(22) Barley, M. H.; Rhodes, M. R.; Meyer, T. J. *Inorg. Chem.* **1987**, *26*, 1746.

0020-1669/88/1327-1198$01.50/0